DOI: 10.1002/chem.201001396

VIP

Atomic-Level Elucidation of the Initial Stages of Self-Assembled Monolayer Metallization and Nanoparticle Formation

John A. Keith and Timo Jacob*[a]

Abstract: The development of high-performance molecular electronics and nanotech applications requires deep understanding of atomic level structural, electronic, and magnetic properties of electrode/molecular interfaces. Recent electrochemical experiments on self-assembled monolayers (SAMs) have identified highly practical means to generate nanoparticles and metal monolayers suspended above substrate surfaces through SAM metallizations. A rational basis why this process is even possible is not yet well-understood. To clarify the initial stages of interface formation during SAM metallization, we used first-principles spin-polarized density functional theory (DFT) calculations to study Pd diffusion on top of 4-mercaptopyridine (4MP) SAMs on Au(111). After distinguishing potential-energy surfaces (PESs) for different spin configurations for transition metal atoms on the SAM, we find adatom diffusion is not possible over the clean 4MP–SAM surface. Pre-adsorption of transition-metal atoms, however, facilitates atomic diffusion that appears to explain multiple reports on experimentally observed island and monolayer formation on top of SAMs. Furthermore, these diffusions most likely occur by moving across low-lying and intersecting PESs of different spin states, opening the possibility of magnetic control over these systems. Vertical diffusion processes were also investigated, and the electrolyte was found to play a key role in preventing metal permeation through the SAM to the substrate.

Keywords: density functional calculations · gold · metal–organic interfaces · monolayers · palladium · self-assembly

Introduction

The performance of nanodevices depends on structural, electronic, and magnetic properties of their comprised materials and interfaces.[1] Accurate and precise characterization of these properties remains a challenge to both theory and experiment, but efforts in this field have still driven creative and elegant nanotechnology studies on electronic and spin transport through systems including a range of single organic molecules to networks of organic layers.[2] Indeed, molecular electronics are "approaching reality",[3] and controlling spin-states of semiconductors has opened the field of molecular spintronics,[4] a field that has recently seen a report of single-molecule magnetic memory.[5] Unfortunately, these applications usually suffer from the difficulty in understanding and controlling the aforementioned properties. Clarification of the nature of metal-organic interfaces[6] and modification of the local density of states at such interfaces is desirable.[7]

One route to highly dense nanodevices is with self-assembled monolayers (SAMs), which have been intensively studied for engineering surfaces with specific properties.[8] When connected to metallic substrates, SAMs show great potential for a variety of new technologies as molecular sensors[9] and molecular electronics.[7,10] Short aromatic SAMs supported on gold have already been used for diverse purposes such as for immobilizing proteins on surfaces[11] and detecting extremely low (ppb) concentrations of metal ions in solutions.[12] The unique conductive properties of short aromatic thiols, such as 4-mercaptopyridine (4MP) (inset, Figure 1), make them promising candidates for SAM metallization, the process of generating a second organic/metal interface in situ.[7,10b]

Notably, vapor metal deposition studies in dry conditions attempting to create an isolated metal layer on top of SAMs have largely been unsuccessful, though with some successes.[13] Kolb and co-workers[7] recently realized a hanging metal overlayer on top of the 4MP–SAM on Au(111) by

[a] Dr. J. A. Keith, Dr. T. Jacob
Institut für Elektrochemie, Universität Ulm
Albert-Einstein-Allee 47, 89081, Ulm (Germany)
Fax: (+49) 731-50-25409
E-mail: timo.jacob@uni-ulm.de

Supporting information for this article is available on the WWW under http://dx.doi.org/10.1002/chem.201001396.

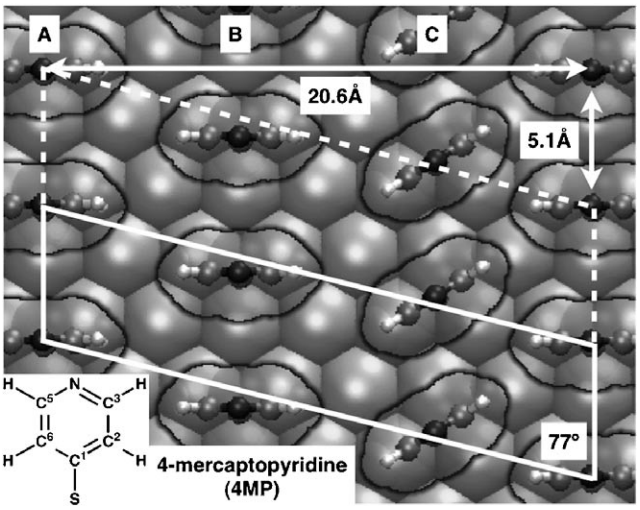

Figure 1. A top-view of the $\sqrt{3}\times7$ 4MP–SAM over-layer on Au(111). Ellipsoids denote 4MP–SAM vdW radii. The solid and dashed parallelograms are the $\sqrt{3}\times7$ and $2\sqrt{3}\times7$ unit cells, respectively. 4MP molecules in molecular row A and B are parallel while those in molecular row C are twisted by 32° with respect to other molecular rows. Inset: The 4-mercaptopyridine molecule (4MP).

means of practical metal deposition techniques in electrochemical cells. They extended this methodology to different metals and different SAMs.[14] They have also generated novel surfaces depositing metals on a SAM which itself is on another SAM[15] and depositing a metal layer on a SAM, which itself is on a metal layer on a SAM.[16]

The mechanism that forms the systems mentioned above are fundamentally different than metal–organic monolayer formation on a surface in which both the SAM and the metals make contact with the substrate.[17] In the cases studied here, metal deposition resulted in 4.9–9.0 nm-sized Pd islands suspended above the SAM. Although these structures require preparation under electrochemical conditions, the metallized surfaces are also stable in air up to 70 °C.[18] Due to its stability, this system could be a useful model for investigating electrode-molecule contacts or tuning the properties of electrochemical interfaces. However, the lack of atomic level understanding of metallization mechanisms, as well as the well-defined structure of the interface, prevents the active control of the structures and properties of such metal-organic-metal interfaces.

Such metal depositions can occur on different SAMs, but the 4MP–SAM on a Au(111) electrode is the most-studied for these systems. Unlike alkane thiols, which are often encountered having a $\sqrt{3}\times\sqrt{3}$ overlayer structure, in situ scanning tunneling microscopy (STM) measurements on 4MP–SAMs characterized different overlayers including the $\sqrt{3}\times1$,[19] $\sqrt{3}\times5$,[20] $\sqrt{3}\times7$,[19] or $\sqrt{3}\times10$[21] periodicities. In preparations using 4MP dimers for the monolayer, the $\sqrt{3}\times7$ structure is predominant. Here, three 4MP molecules reside in the unit cell: two molecules are parallel to each other and the third twisted out of the parallel plane by ≈30° (see Figure 1). Each SAM molecule is distanced at least 5.1 Å apart from each of the others,[21] though note that this is almost twice the nearest neighbor distance in bulk Pd (calculated = 2.772 Å, experimental[22] = 2.751 Å), the metal used in a previous study.[7] The fact that each 4MP monomer is quite far (>5 Å) from its next nearest neighbor indicates a non-trivial diffusion mechanism is in play.

Kučera and Groß have performed DFT calculations on three high coverage 4MP–SAM structures, the $\sqrt{3}\times\sqrt{3}$, $\sqrt{3}\times5$, and $\sqrt{3}\times7$ overlayers and compared them to a low-coverage 3×3 structure.[23] In the experimentally accessible region of the surface phase diagram, the surface free energy was lowest for the $\sqrt{3}\times7$ overlayer, but the 3×3 and $\sqrt{3}\times\sqrt{3}$ structures were only slightly less stable (<10 meV Å^{-2}). The small energy differences suggest that any or a combination of these structures may be present under ambient conditions. Although different SAM structures may coexist, the $\sqrt{3}\times7$ structure is the most interesting, as it has the highest stability and shares similar structural characteristics with the $\sqrt{3}\times\sqrt{3}$, $\sqrt{3}\times5$, and $\sqrt{3}\times10$ overlayers.

Although no mechanism has yet explained how these islands form, several mechanistic details have already been presented. First, XPS measurements have determined that Pd islands are in a zero-valent state,[14a] so Pd^{II} is expected to be fully reduced to Pd^0. Second, experiments with 2-mercaptopyridine, a chemically identical molecule with its N atom facing away from the electrolyte, result in no Pd deposition,[14b] so nitrogen-containing groups appear to facilitate metal reduction. Finally, cyclic voltammetry (CV) measurements show a deposition charge of 150 μC cm^{-1}, roughly corresponding to ≈1/3 of a monolayer (ML) of Pd. This is a slightly higher coverage for the 4MP–SAM alone according to CV measurements (≈1/4 ML)[19] and STM experiments (≈1/3–1/5 ML).[24] Thus, Pd is likely reduced in close to a 1:1 ratio with respect to 4MP–SAM molecules.

Combining these observations, a metallization mechanism can be hypothesized. Metallization probably begins by Pd^{II} ions from the electrolyte binding to all available SAM molecules and then reducing to Pd^0 on a 4MP monomer. This would result in a vast arrangement of Pd^0 atoms on each SAM molecule. Since metal islands with sizes of 4–9 nm have been characterized experimentally immediately after deposition, a diffusion mechanism must allow the atoms to aggregate into nanoscale islands. A simple diffusion mechanism, however, relies on a counterintuitive expectation that Pd easily diffuses across SAM molecules, which are 5.1 Å apart and have nitrogen-atom end groups that certainly will bind to Pd. We address this particular question by investigating vertical and horizontal Pd diffusion pathways on the most probable 4MP–SAM surfaces: the $\sqrt{3}\times7$ and $\sqrt{3}\times\sqrt{3}$ structures. The results and conclusions on the more complicated former structure are discussed here, and those of the latter more-compact configuration (which are qualitatively similar) have previously been reported.[25]

Results and Discussion

Summarized calculation details can be found in the Computational Methods section. Pd adsorption with different coverages was studied on both $\sqrt{3}\times7$ and $2\sqrt{3}\times7$ surface unit cells. The latter model involved around 150 atoms and eliminated periodic constraints on the SAM. Optimization of the $\sqrt{3}\times7$ 4MP–SAM led to structural parameters of $a=5.1$, $b=20.6$ Å, and $\gamma=77°$ in full agreement with the experimentally characterized structure: $a=4.7\pm0.5$ Å, $b=22\pm3$ Å, $\gamma=75\pm3°$.

Kučera and Groß find 4MP monomers bind most strongly at binding sites between bridge and face-centered cubic (fcc) sites, though binding at fcc sites is only <0.04 eV less favored.[23] In contrast, we find 4MP monomers bind 0.02 eV stronger at fcc sites than these pseudo-bridge sites. Given the narrow difference between these binding energies and the inherent differences in DFT calculations, both sites should be considered as feasible binding sites. We also find a very small energy difference between $\sqrt{3}\times7$ structures containing two 4MP groups at fcc sites and one at a hexagonal close packed (hcp) site compared to one on an fcc site and two on hcp sites. The former surface is favored by 0.11 eV, and all reported data are based on this surface.

We first calculated the rotational freedom of the 4MP–SAM in the $\sqrt{3}\times7$ structure before Pd deposition. By rotating 4MP monomers around the axis normal to the surface, we obtained energy profiles with respect to the torsion angle. Due to the relatively weak intermolecular interactions, each 4MP molecule displays a wide range of torsional freedom ($-60<\varphi<60°$) for which the energy is always <0.06 eV with respect to its preferred orientation. Since it is known that density functionals usually do not accurately describe energy contributions from van der Waals (vdW) π–π interactions, we also performed ab initio calculations using pyridine dimers as a model system (see supporting information). Interestingly, we found very small energy differences (≤0.03 eV) between DFT-PBE and CCSD(T) energy profiles when pyridines were simultaneously rotated at positions 5.1 Å apart (the calculated 4MP–4MP distance in the $\sqrt{3}\times7$ structure). Since the CCSD(T) calculated optimum π–π stacking distance for a pyridine dimer is 3.80 Å, we conclude 4MP groups are too far apart for vdW interactions to play an important role in 4MP–SAM assembly on Au(111). Rather, binding effects on the Au(111) surface likely dominate once the surface is assembled. The shallow energy profile within a range of $\approx120°$ suggests 4MP-groups will concertedly rotate when motivated to do so. Of course, the presence of the electrolyte or an electrode potential might influence this behavior.

We then studied the adsorption of atomic Pd at various sites[26] and used these data to generate corresponding potential energy surfaces shown in Figure 2 a–c. Before discussing these points in detail, however, we investigated vertical diffusion through the SAM to the gold surface from points **a** and **c** denoted in Figure 2 to understand why metal deposition under electrochemical conditions is more successful

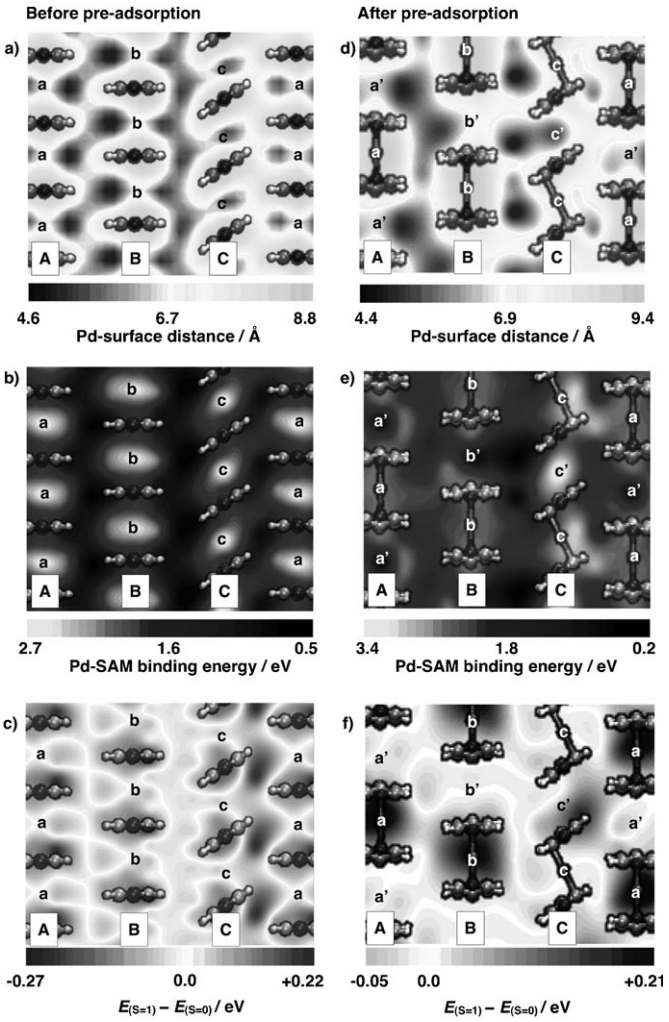

Figure 2. Potential energy surfaces for atomic Pd diffusing across the clean $2\sqrt{3}\times7$ 4MP–SAM (left) and across the $2\sqrt{3}\times7$ 4MP–SAM with three pre-adsorbed Pd atoms filling unique sites a, b, and c (right). Labels correspond to positions on the SAM referenced in Tables 1 and 2. The different figures show the Pd-surface height profiles, a) and d), the Pd–SAM binding energy profiles, b) and e), and the difference between $S=1$ and $S=0$ energies, c) and f). Positive values denote relative preference towards $S=1$ spin states.

than vapor deposition. Indeed, we found single-atom vertical diffusion to be a largely facile process with a maximum barrier of only <0.3 eV, explaining why under gas-phase conditions Pd permeates the SAM. However, since successful metallization techniques for this system required electrochemical conditions, we considered vertical diffusion of an aquo-complex of Pd with one and two H_2O molecules. The new barriers are substantially higher (>0.5 eV), and thus it can be rationalized that the solvent plays a key role in preventing permeation of the metal through the SAM.

Due to the importance of distinguishing specific electronic and spin configurations of small metal clusters,[27] we also evaluated the $S=1$ and $S=2$ configurations for the surface unit cell. As expected, binding of Pd in a $S=2$ configuration was always significantly higher in energy (≈0.4 eV), howev-

er, $S=0$ and $S=1$ energy surfaces frequently intersect. Therefore, it seems that the substrate induces spin-flips within the electronic structure of the diffusing Pd. This process can be rationalized as a preference for $S=0$ states whenever a relatively strong Pd–SAM interaction is at play, usually closer to the Au surface. Otherwise, there is a preference for $S=1$ states stabilized by the vast array of π systems in the 4MP–SAM. This already shows the complexity of the present system, and spin-polarized calculations of different electronic configurations are required to obtain the lowest energy pathways for Pd adatom diffusion.

The first potential-energy surfaces (PES; Figure 2a–c) correspond to horizontal diffusion of Pd on a clean 4MP–SAM with a $2\sqrt{3}\times7$ unit cell (Figure 1). At each position, we constrained the x and y coordinates of the diffusing atom, while allowing all other atoms (apart from the bottom two Au layers) to relax. For the $S=1$ PES, we allowed the geometry to relax starting from the optimized $S=0$ state, even though the calculated forces at the $S=0$ optimized geometry were typically small. These combined results yielded the optimal Pd-surface distance (Figure 2a), binding energy (Figure 2b), and the difference between $S=0$ and $S=1$ energy surfaces (Figure 2c) for Pd at all positions above the 4MP–SAM.

The height profile in Figure 2a shows that Pd always prefers positions relatively far above the substrate surface. For reference, the 4MP–SAM extends to 6.5 Å above the surface. The highest points on the PES correspond to adsorptions directly on top of 4MP molecules, whereby the Pd resides around 8.8 Å above the Au surface. In comparison, the lowest points are exactly between 4MP molecules, in which Pd resides in the π systems between two pairs of SAM molecules being located ≈4.6 Å above the Au surface.

The binding energy profile, Figure 2b, reports the strongest binding regions either at a $S=0$ or $S=1$ state. Binding energies for this study are found in Table 1. We find Pd prefers binding between the N atoms of the SAM molecules (molecular row A: 2.59 eV, B: 2.53 eV, C: 2.68 eV) rather than on top of the nitrogen atoms of the pyridines (≈1.70 eV). The twisted SAM molecules in molecular row C involve slightly different binding than those in molecular rows A or B and deserve special mention. Here, Pd–SAM binding involves the π systems of a pair of SAM molecules. Specifically, the π bond between the C2 and C3 atoms of any twisted SAM are aligned with the π bond the C5 and C6 atoms of the adjacent SAM molecule. Coincidentally, the calculated binding energy for a Pd atom is only ≈0.1 eV stronger than that in the sites in molecular rows A and B. The strong binding has profound implications for atomic diffusion. High diffusion barriers in the range of 0.95–1.64 eV were found (Table 1) for hopping between stable surface sites. These are too high to be considered feasible diffusion barriers, even when including zero-point energies, as well as thermal and entropic energy contributions, which we estimated to be no more than 0.3 eV.

Table 1. Binding energies and process barrier heights for diffusion processes on a clean 4MP–SAM surface (before pre-adsorption). All energies in are eV.

Site	E_{bind}	Barrier to product sites					
		a	**b**	**c**	**a′**	**b′**	**c′**
a	2.59	–	1.61	1.21	0.99	1.61	1.21
b	2.53	1.55	–	1.64	1.55	0.95	1.64
c	2.68	1.30	1.61	–	1.30	1.61	1.02
a′	2.59	0.99	1.61	1.21	–	1.61	1.21
b′	2.53	1.55	0.95	1.64	1.55	–	1.64
c′	2.68	1.30	1.61	1.02	1.30	1.61	–

Since the experimental system is in contact with an aqueous electrolyte of low ion concentration, we also investigated the role of water on atomic metal diffusion. Without the substrate, Pd to binds two water molecules with a total strength of 0.45 eV. Since the absolute binding energy of water to Pd may be altered over the course of diffusion, we then recalculated the diffusion barriers with two water molecules coordinated to Pd. Nevertheless, the lower diffusion barriers for the $Pd(H_2O)_2$ complex were in the range of 0.7–1.4 eV, which still is too high for significant Pd diffusion.

Finally, Figure 2c shows the difference between $S=1$ and $S=0$ energy surfaces for the adsorbed Pd atom. Here, green regions indicate Pd adsorption is preferred with $S=1$, while red regions show adsorption is preferred with $S=0$ adsorption. Even though spin crossings between $S=0$ and $S=1$ states are expected to be possible and occur, the overall energy differences along possible diffusion pathways are relatively small (see scale of Figure 2c). Nevertheless, this result shows that spin-polarized calculations are required to obtain minimum energy states for single atom diffusion on these SAMs.

Our studies on the diffusion of a single Pd atom per $2\sqrt{3}\times7$ unit cell showed that the energy barriers are too high to overcome under ambient conditions. Even the presence of an electrolyte, which most likely would lead to the coordinative complexation of water molecules to Pd, does not reduce the barriers enough to make diffusion become feasible under ambient conditions. Thus, one would expect that after the first stages of reduction Pd atoms would reside between 4MP molecules.

In the next step, we considered atomic diffusion on top of a 4MP–SAM that already had reduced Pd atoms occupying the most stable sites.[28] In order to allow for enough rearrangement of the SAM upon Pd adsorption, only three of the six possible strongly binding positions (**a**, **b**, and **c** in Figure 2b, leading to the structure shown in Figure 2d) between pyridine molecules were occupied. Under this configuration, 4MP–SAM molecules have slightly relaxed in order to maximize overlap of bonding orbitals with nearby Pd atoms. As for the system before pre-adsorption, Pd adsorption has been studied at various sites of the $2\sqrt{3}\times7$ unit cell to yield the height profile and energy surfaces (Figure 2d–f). Binding energies and barrier heights for these processes are reported in Table 2.

The height profile again indicates that Pd always resides above the Au substrate. However, now the atom prefers the position on top of the N atom of the pyridine molecule. At

Table 2. Binding energies and barrier heights for diffusion processes on a 4MP–SAM surface containing three pre-adsorbed Pd atoms. All energies are in eV.

Site	E_{bind}	Barrier to product sites					
		a	**b**	**c**	**a′**	**b′**	**c′**
a	2.58	–	0.46	0.22	0.18	0.46	0.30
b	2.67	0.55	–	0.90	0.55	0.35	0.90
c	2.99	0.63	1.22	–	0.59	1.22	0.72
a′	2.58	0.18	0.46	0.18	–	0.46	0.30
b′	2.67	0.55	0.35	0.90	0.55	–	0.90
c′	3.41	1.13	1.64	1.13	1.13	1.64	–

the highest point (9.4 Å above the surface) Pd is on a pre-adsorbed Pd atom, and the lowest point (4.4 Å) is now between SAM molecules in molecular rows B and C.

The binding-energy profile (Figure 2e) shows a dramatic difference from the clean 4MP–SAM surface (Figure 2b). Absolute binding energies near the pre-adsorbed Pd atoms in molecular rows A and B are comparable as before (2.57 and 2.67 eV, respectively); however, adsorption at regions of molecular row C is increased to as much as 3.39 eV due to much more complimentary binding between the π systems of the twisted SAM molecules. Importantly, now diffusion barriers to almost anywhere on the complete surface are reduced to values between 0.2–0.6 eV when accounting for step-wise processes. Assuming a similar effect from Pd–electrolyte (i.e., water) interactions as reported earlier, diffusion barriers across this surface treated with pre-adsorbed Pd should reduce even further. Consequently, we find strong evidence that the SAM structure due to pre-adsorbed Pd facilitates atomic Pd diffusion during the initial stages of metal/organic interface formation.

Interestingly, the difference between the $S=0$ and $S=1$ energy surfaces (Figure 2f) is qualitatively different from that of the clean 4MP–SAM surface (Figure 2c). Instead of the $S=1$ and $S=0$ surfaces interchanging, the presence of additional Pd atoms on the SAM reduces the energy of the $S=1$ surface such that it is almost always preferred. This also agrees with the fact that Pd-dimers assume triplet spin-configurations. While the overall energy differences between $S=1$ and $S=0$ states are again quite small, we caution that realistic cluster formation studies on these systems require careful attention to the spin configuration of the diffusing Pd atom. As our studies explain the diffusion of Pd on the 4MP–SAM, it is reasonable to expect a standard Ostwald ripening mechanism finally leading to the formation of small Pd islands or even a completely metallized SAM.

Conclusion

We have used first principles DFT to elucidate the initial stages of SAM metallization using Pd on 4MP–SAM on Au(111) as a model. Although recent electrochemical studies have indicated a highly practical approach to generating well-dispersed nanoparticles and metal monolayers suspended above SAMs, several questions remained regarding how this is possible. First, we find metal complexation with solvent explains why vapor deposition studies differ from metal deposition studies on related systems under electrochemical conditions.

Furthermore, metal atoms should not be capable of diffusing across a clean 4MP–SAM, even after accounting for spin crossings and interactions with the electrolyte. However, pre-adsorbed Pd atoms lead to structural and electronic modifications of the 4MP–SAM, finally promoting atomic diffusion that expectedly would lead to island formation on top of the SAM and eventually complete metallization. This strong binding of metal atoms to the SAM may also explain why these nanoparticles remain stable even under harsh electrochemical conditions.

Our results also show that both $S=0$ and $S=1$ spin-configurations are continually in play during these initial diffusions. Qualitatively similar observations from a study on the $\sqrt{3}\times\sqrt{3}$ structure[25] suggest these conclusions are transferable to moderately higher SAM coverages and different surface unit-cell structures.

Computational Methods

All periodic density functional theory (DFT) calculations were performed with SeqQuest,[29] which is based on localized basis sets represented by linear combinations of contracted Gaussian functions (at the "double-zeta plus polarization" level). We employed the PBE-GGA[30] exchange-correlation functional in tandem with standard (nonlocal) norm-conserving pseudopotentials.[31]

Integrations in reciprocal space were performed with a converged Brillouin zone sampling of 8×2 $\boldsymbol{k}$-points per $\sqrt{3}\times7$ unit cell. Our studies represented the Au(111) surface as a three-layer slab, in which the lowest two layers were fixed to the calculated bulk structure, while the top-most Au layer, the 4MP–SAM molecules, and the adsorbed Pd atoms were allowed to freely optimize their geometry (up to $<0.1\,\mathrm{eV\,Å})^{-1}$. Convergence tests indicated the binding energy of the 4MP–SAM as well as a Pd-atom on top of the 4MP–SAM on 3, 4, and 5-layered slabs differed by ≤0.015 eV. Thus, we deemed the 3-layer slab to be sufficiently converged for this study.

Higher level ab initio calculations (i.e. MP2, MP4, CCSD(T)) were run with the MOLPRO code using the 6-31G**$^{++}$ basis set level.[32]

Acknowledgements

We thank Axel Groß, Jan K. Kučera, and Dieter Kolb for helpful discussions. Support from the Alexander von Humboldt Foundation (AvH), the Fonds der Chemischen Industrie (FCI), and the Deutsche Forschungsgemeinschaft (DFG) within the Emmy-Noether Program is gratefully acknowledged, as well as the bwGRiD project[33] for computational resources.

[1] *Springer Handbook of Nanotechnology*, 2nd ed. (Ed.: B. Bhushan), Springer, Heidelberg, **2006**.

[2] a) P. Seneor, A. Bernand-Mantel, F. Petroff, *J. Phys. Condens. Matter* **2007**, *19*, 165222; b) B. Ulgut, H. D. Abruna, *Chem. Rev.* **2008**, *108*, 2721–2736.

[3] J. M. Seminario, *Nat. Mater.* **2005**, *4*, 111–113.

[4] A. Fert, *Rev. Mod. Phys.* **2008**, *80*, 1517–1530.

[5] M. Mannini, F. Pineider, P. Sainctavit, C. Danieli, E. Otero, C. Sciancalepore, A. M. Talarico, M.-A. Arrio, A. Cornia, D. Gatteschi, R. Sessoli, *Nat. Mater.* **2009**, *8*, 194–197.
[6] K. W. Hipps, *Science* **2001**, *294*, 536–537.
[7] H.-G. Boyen, P. Ziemann, U. Wiewald, V. Ivanova, D. M. Kolb, S. Sakong, A. Gross, A. Romanyuk, M. Büttner, P. Oelhafen, *Nat. Mater.* **2006**, *5*, 394–399.
[8] a) E. Ito, J. Noh, M. Hara, *Chem. Phys. Lett.* **2008**, *462*, 209–212; b) M. Lazzari, C. Rodriguez-Abreu, J. Rivas, M. A. López-Quintela, *J. Nanosci. Nanotechnol.* **2006**, *6*, 892–905; c) J. C. Love, L. A. Estroff, J. K. Kriebel, R. G. Nuzzo, G. M. Whitesides, *Chem. Rev.* **2005**, *105*, 1103–1169; d) M. Mrksich, *ACS Nano* **2008**, *2*, 7–18; e) A. Ulman, *Chem. Rev.* **1996**, *96*, 1533–1554.
[9] X. Dong, Y. Xia, G. Zhu, B. Zhang, *Nanotechnology* **2007**, *18*, 395502–395508.
[10] a) A. Gross, *J. Comput. Theor. Nanosci.* **2008**, *5*, 894–922; b) O. Shekhah, C. Busse, A. Bashir, F. Turcu, X. Yin, P. Cyganik, P. Birkner, A. Schuhmann, W. Wöll, *Phys. Chem. Chem. Phys.* **2006**, *8*, 3375–3378.
[11] a) F. A. Armstrong, H. A. O. Hill, N. J. Walton, *Acc. Chem. Res.* **1998**, *31*, 407–413; b) M. J. Eddowes, H. A. O. Hill, *J. Am. Chem. Soc.* **1979**, *101*, 4461–4464.
[12] a) I. Rubinstein, S. Steinberg, Y. Tor, A. Shanzer, J. Sagiv, *Nature* **1988**, *332*, 426–429; b) I. Turyan, D. Mandler, *Anal. Chem.* **1997**, *69*, 894–897.
[13] a) G. C. Herdt, A. W. Czanderna, *J. Vac. Sci. Technol. A* **1999**, *17*, 3415–3418; b) D. R. Jung, A. W. Czanderna, G. C. Herdt, *J. Vac. Sci. Technol. A* **1996**, *14*, 1779–1787; c) H. Haick, O. Niitsoo, J. Ghabboun, D. Cahen, *J. Phys. Chem. A* **2007**, *111*, 2318–2329; d) H. Haick, D. Cahen, *Prog. Surf. Sci.* **2008**, *83*, 217–261; e) M. J. Preiner, N. A. Melosh, *Appl. Phys. Lett.* **2008**, *92*, 213301.
[14] a) T. Baunach, V. Ivanova, D. M. Kolb, H.-G. Boyden, P. Ziemann, M. Büttner, P. Oelhafen, *Adv. Mater.* **2004**, *16*, 2024–2028; b) V. Ivanova, T. Baunach, D. M. Kolb, *Electrochim. Acta* **2005**, *50*, 4283–4288; c) M. Manolova, V. Ivanova, D. M. Kolb, H.-G. Boyden, P. Ziemann, M. Büttner, A. Romanyuk, P. Oelhafen, *Surf. Sci.* **2005**, *590*, 146–153; d) M. Manolova, M. Kayser, D. M. Kolb, H.-G. Boyen, P. Ziemann, D. Mayer, A. Wirth, *Electrochim. Acta* **2007**, *52*, 2740–2745.
[15] M. Manolova, H.-G. Boyen, J. Kučera, A. Groß, A. Romanyuk, P. Oelhafen, V. Ivanova, D. M. Kolb, *Adv. Mater.* **2008**, *20*, 320–324.
[16] F. Eberle, M. Manolova, D. Kolb, M. Saitner, H.-G. Boyen, J. Kučera, A. Groß, A. Romanyuk, P. Oelhafen, *Angew. Chem.* **2009**, *121*, 6732–6757; *Angew. Chem. Int. Ed.* **2009**, *49*, 341–345.
[17] H.-M. Zhang, W. Zhao, Z.-X. Xie, L.-S. Long, B.-W. Mao, X. Xu, L.-S. Zheng, *J. Phys. Chem. C* **2007**, *111*, 7570–7573.
[18] Communication with D. M. Kolb.
[19] W. P. Zhou, T. Baunach, V. Ivanova, D. M. Kolb, *Langmuir* **2004**, *20*, 4590–4595.
[20] a) T. Sawaguchi, F. Mizutani, I. Taniguchi, *Langmuir* **1998**, *14*, 3565–3569; b) L. J. Wan, Y. Hara, H. Noda, M. Osawa, *J. Phys. Chem. B* **1998**, *102*, 5943–5946.
[21] T. Baunach, V. Ivanova, D. A. Scherson, D. M. Kolb, *Langmuir* **2004**, *20*, 2797–2802.
[22] C. N. Rao, K. K. Rao, *Can. J. Phys.* **1964**, *42*, 1336–1342.
[23] J. Kučera, A. Groß, *Langmuir* **2008**, *24*, 13985–13992.
[24] We define coverage, $\theta = n/a$, in which n is the number of species on the surface and a is the number of available surface atoms within the unit cell. For the 4MP–SAM on Au(111), the $\sqrt{3}\times\sqrt{3}$ contains 1 SAM molecule and 3 surface atoms, thus leading to a coverage of 1/3 ML. The $\sqrt{3}\times 7$ surface structure has 3 SAM molecules and 14 atoms, so its coverage is 3/14–1/5 ML.
[25] J. A. Keith, T. Jacob, *Electrochim. Acta.* **2010**, DOI: 10.1016/j.electacta.2010.04.027.
[26] The $2\sqrt{3}\times 7$ surface structure contains 28 surface atoms, so the corresponding coverage is 1/28 ML.
[27] a) P. Nava, M. Sierka, R. Ahlrichs, *Phys. Chem. Chem. Phys.* **2003**, *5*, 3372–3381; b) J. Rogan, G. García, J. A. Valdivia, W. Orellana, A. H. Romero, R. Ramírez, M. Kiwi, *Phys. Rev. B* **2005**, *72*, 115421.
[28] The $2\sqrt{3}\times 7$ surface structure contains 28 surface atoms, so the corresponding coverage is $4/28 = 1/7$ ML.
[29] C. Verdozzi, P. A. Schultz, R. Wu, A. H. Edwards, N. Kioussis, *Phys. Rev. B* **2002**, *66*, 125408.
[30] J. P. Perdew, K. Burke, M. Ernzerhof, *Phys. Rev. Lett.* **1996**, *77*, 3865–3868.
[31] a) D. R. Hamann, *Phys. Rev. B* **1989**, *40*, 2980–2987; b) S. G. Louie, S. Froyen, M. L. Cohen, *Phys. Rev. B* **1982**, *26*, 1738–1742.
[32] MOLPRO, version 2006.1, a package of ab initio programs, H.-J. Werner, P. J. Knowles, R. Lindh, F. R. Manby, M. Schütz, Cardiff, **2006**.
[33] bwGRiD (http://www.bw-grid.de), member of the German D-Grid initiative funded by the Ministry for Education and Research (Bundesministerium für Bildung und Forschung) and the Ministry for Science Research and Arts Baden-Württemberg (Ministerium für Wissenschaft, Forschung und Kunst Baden-Württemberg).

Received: May 20, 2010
Published online: September 15, 2010

